# Ba₂[Ni₃N₂]: A Low-Valent Nitridonickelate—Synthesis, Crystal Structure, and Physical Properties

## Akash Mehta, Peter Höhn,* Walter Schnelle, Vivien Petzold, Helge Rosner, Ulrich Burkhardt, and Rüdiger Kniep[a]

**Abstract:** The ternary alkaline-earth nitridonickelate $Ba_2[Ni_3N_2]$ ($Ba_2[Ni^I_2 Ni^0 N_2]$) was prepared by the reaction of mixtures of $Ba_2N$ and Ni in nitrogen gas of ambient back-pressure at 1173 K. The crystal structure determined by X-ray single-crystal and powder diffraction methods as well as from neutron diffraction data at various temperatures between 2 and 298 K is orthorhombic ($Cmca$ (no. 64), 298 K: $a = 715.27(18)$ pm, $b = 1032.99(21)$ pm, $c = 740.12(20)$ pm) and provides the first example of a nitridonickelate with a two-dimensional complex anion. The Ni(2) atom is described with a split position and the corresponding superstructure variants are investigated by theoretical full-potential nonorthogonal

**Keywords:** magnetic properties · mixed-valent compounds · nitridonickelates · structure elucidation

local-orbital calculations (FPLO). The average oxidation state of Ni in $Ba_2[Ni_3N_2]$ is $+0.67$, the lowest average value observed in nitridonickelates so far. Investigations of the physical properties demonstrate that $Ba_2[Ni_3N_2]$ acts as a "poor" metal with a large resistivity of $\approx 2.7$ mΩ cm at 300 K and exhibits low-dimensional magnetism with antiferromagnetic ordering at $T \approx 90$ K. XAS spectra correspond with low-valent Ni states.

## Introduction

The chemistry of nitridometalates is an area of rapid development and increasing diversity.[1] Nitridonickelates of lithium and alkaline-earth metals have been thoroughly investigated since the pioneering work of Robert Juza.[2] Common structural features of nitridonickelates are infinite $[NiN_{2/2}]$ chains with nickel coordinated in an almost linear (twofold) fashion by nitrogen and short Ni–N contacts (179–187 pm[3–12]). Nitridonickelates are characterized by exceptionally low oxidation states of nickel with the most common oxidation state Ni$^I$, as observed in the ternary compounds AE[NiN] (AE (alkaline-earth metal) = Ca,[3,4] Sr,[5,6] Ba[7]). Mixed-valent Ni$^{0,I}$ is observed in $Ba_2(Ba_6N)[NiN]_6$[8] and $Li_3Sr_3Ni_4N_4$[9] as well as in $Ba_2[(Li_{1-x}Ni_x)Ni_2N_2]$,[10] a solid solution variant of the title compound $Ba_2[Ni_3N_2]$ with "$Ba_2[LiNi_2N_2]$", but no physical property investigations on any of the mixed-valent compounds have been reported up to now. Higher oxidation states (up to Ni$^{II}$) were reported in

$Li_5[NiN_3]$,[11,12] Li[NiN],[12] and $Sr_2[NiN_2]$,[13] but at least the latter compound remains doubtful.[14]

Here we report on the synthesis, structure, and physical properties of $Ba_2[Ni_3N_2]$,[15] the first mixed low-valency nitridonickelate with a two-dimensional metal–nitrogen anionic network.

## Results and Discussion

**Crystal structure**: $Ba_2[Ni_3N_2]$ crystallizes with the orthorhombic space group $Cmca$ (no. 64, $a = 715.27(18)$ pm, $b = 1032.99(21)$ pm, $c = 740.12(20)$ pm, $V = 546.9(4) \times 10^6$ pm$^3$. Both room-temperature powder X-ray diffraction data and neutron diffraction data correspond well with these values within the standard deviation. In a first single-crystal data refinement, the anisotropic displacement parameters for the Ni(2) atom show an anomaly in $U_{11}$, resulting in a prolate (cigar-shaped) thermal displacement ellipsoid. A subsequent refinement of the Ni(2) atom as a split position gives rise to "normal" displacement parameters with the occupation parameter remaining constant within the standard deviation, whereas a change to a lower symmetry space group (e.g. $C222_1$ (no. 20), $C2ca$ (no. 41), $Pbcb$ (no. 54), $Pbna$ (no. 60)) does not improve the model. This behavior is discussed in depth later taking low-temperature data into consideration.

[a] Dipl.-Ing. A. Mehta, Dr. P. Höhn, Dr. W. Schnelle, V. Petzold,
Dr. H. Rosner, Dr. U. Burkhardt, Prof. Dr. R. Kniep
Max-Planck-Institute for Chemical Physics of Solids
Nöthnitzer Strasse 40, 01187 Dresden (Germany)
Fax: (+49) 351-4646-2260
E-mail: hoehn@cpfs.mpg.de

WILEY InterScience®
DISCOVER SOMETHING GREAT

**These are not the final page numbers!** ⌐⌐

Table 1. Crystallographic data for $Ba_2[Ni_3N_2]$ at 293, 200, and 100 K from single-crystal X-ray diffraction data.[a]

| Temperature of measurement | 293 K | 200 K | 100 K |
|---|---|---|---|
| crystal system | orthorhombic | orthorhombic | orthorhombic |
| space group | $Cmca$ (no. 64) | $Cmca$ (no. 64) | $Cmca$ (no. 64) |
| $a$ [pm] | 715.27(18) | 712.47(6) | 712.55(7) |
| $b$ [pm] | 1032.99(21) | 1027.01(10) | 1026.11(11) |
| $c$ [pm] | 740.12(20) | 736.40(7) | 736.19(8) |
| cell volume [$10^6$ pm$^3$] | 546.9(4) | 538.9(2) | 538.3(2) |
| $Z$ | 4 | 4 | 4 |
| $\rho_{calcd}$ [g cm$^{-3}$] | 5.816 | 5.901 | 5.909 |
| crystal color, habit | shiny black, irregular | shiny black, irregular | shiny black, irregular |
| crystal size [mm$^3$] | $0.1\times0.1\times0.1$ | $0.1\times0.1\times0.1$ | $0.1\times0.1\times0.1$ |
| $\mu(Ag_{K\alpha})$ [mm$^{-1}$] | 12.715 | 12.90 | 12.92 |
| $2\theta$ range [°] | 6.22–47.60 | 6.26–55.54 | 6.26–55.70 |
| diffractometer | STOE IPDS | STOE IPDS | STOE IPDS |
| radiation, wavelength [Å] | X-ray, 0.56087 | X-ray, 0.56087 | X-ray, 0.56087 |
| monochromator | graphite | graphite | graphite |
| scan mode | $\Delta\varphi=0.8°$ | $\Delta\varphi=0.8°$ | $\Delta\varphi=0.8°$ |
| measured reflections | 3196 | 4310 | 4422 |
| independent reflections | 456 | 679 | 692 |
| observed reflections [$F_o>4\sigma(F_o)$] | 413 | 636 | 647 |
| $R_{int}$ | 0.0270 | 0.0286 | 0.0309 |
| structure solution method | direct methods | direct methods | direct methods |
| program for structure solution | SHELXS97[24] | SHELXS97[24] | SHELXS97[24] |
| program for structure refinement | SHELXS97[24] | SHELXS97[24] | SHELXS97[24] |
| number of parameters | 24 | 24 | 24 |
| goodness-of-fit on $F^2$ | 1.018 | 1.177 | 1.174 |
| $R1$ [$F_o>4\sigma(F_o)$] | 0.0118 | 0.0164 | 0.0168 |
| $wR2$ | 0.0223 | 0.0335 | 0.0325 |
| $R1$ (all data) | 0.0152 | 0.0189 | 0.0197 |
| $wR2$ | 0.0229 | 0.0341 | 0.0332 |
| residual electron density [e×$10^{-6}$ pm$^{-3}$] | 0.59/−0.47 | 1.22/−0.99 | 1.23/−0.99 |

[a] Further details of the crystal structure investigations can be obtained from the Fachinformationszentrum Karlsruhe, 76344 Eggenstein–Leopoldshafen, Germany, (fax: (+49) 7247-808-666; e-mail: crysdata@fiz.karlsruhe.de) on quoting the depository numbers CSD-415467 (293 K), CSD-415468 (200 K), and CSD-415469 (100 K), respectively.

Table 1 shows crystallographic and refinement data; positional and displacement parameters are given in Tables 2

**Abstract in German:** *Das ternäre Nitridonickelat $Ba_2[Ni_3N_2]$ ($Ba_2[Ni^I_2Ni^0N_2]$) wurde aus $Ba_2N$ und Ni im Stickstoffstrom bei 1173 K dargestellt. Die mit Einkristall- und Pulver-Röntgenbeugungsmethoden sowie Neutronenbeugungsdaten bei verschiedenen Temperaturen zwischen 2 und 298 K bestimmte Kristallstruktur ist orthorhombisch (Cmca (Nr. 64), $a=715.27(18)$ pm, $b=1032.99(21)$ pm, $c=740.12(20)$ pm) und das erste Beispiel für ein ternäres Nitridonickelat mit einem zweidimensionalen komplexen Anion. Ni(2) wird als Splitposition beschrieben, entsprechende Überstrukturvarianten werden mittels theoretischer Rechnungen (full-potential nonorthogonal local-orbital, FPLO) überprüft. Die mittlere Oxidationszahl von Ni in $Ba_2[Ni_3N_2]$ ist +0.67, der niedrigste Mittelwert, der bisher in Nitridonickelaten beobachtet wurde. Physikalische Messungen zeigen, dass $Ba_2[Ni_3N_2]$ ein "schlechtes Metall" ist mit einem großen spezifischen Widerstand von $\approx 2.7$ $m\Omega$ cm bei 300 K. Es weist Anzeichen von niedrigdimensionalem Magnetismus mit einer antiferromagnetischen Ordnung bei $T\approx 90$ K auf. XAS-Spektren stehen mit niedervalenten Ni-Zuständen im Einklang.*

and 3. Selected interatomic distances and angles are given in Table 4.

The predominant features of the crystal structure of $Ba_2[Ni_3N_2]$ (Figure 1) are infinite two-dimensional (2D) puckered layers $^2_\infty[Ni_3N_2^{4-}]$ (see Figure 2a), stacked in an ···AB··· sequence along the [010] direction (see Figure 2b). The two symmetry-independent nickel atoms are coordinated in a nearly linear fashion by nitrogen, and the bond lengths ($d(Ni(1)-N)=179.4(1)$ pm, $d(Ni(2)-N)=187.1(2)$ pm) are within the range observed in other nitridonickelates (Ba-[NiN]: $d(Ni-N)=180.1$ pm;[7] $Ba_2(Ba_6N)[NiN]_6$: $d(Ni-N)=179.22$ pm;[8] Ca[NiN] $d(Ni-N)=179.0(4)$ pm;[3] Sr[NiN] $d(Ni-N)=183.6$ pm[6]). Ni(1)−N bond lengths are significantly shorter than the Ni(2)−N bond lengths. The N atom is coordinated by three Ni and three Ba atoms in a distorted octahedron. Ba is coordinated in a distorted trigonal-planar arrangement by three N atoms, two of them belonging to the same $^2_\infty[Ni_3N_2^{4-}]$ layer and one to the neighboring layer. The Ba−N bond lengths ($d(Ba-N)=284.4(2)$ pm) correspond well with data for other barium nitridonickelates (Ba-[NiN]: $d(Ba-N)=288.05$ pm;[7] $Ba_2(Ba_6N)[NiN]_6$: $d(Ba-N)=299.71$ pm[8]). The $^2_\infty[Ni_3N_2^{4-}]$ network consists of Ni(1)−N chains that run along the [100] direction. Whereas the Ni(1) atom is nearly linearly coordinated by the N atom ($\sphericalangle$N-Ni(1)-N = 179.30(1)°), the $\sphericalangle$Ni(1)-N-Ni(1) angle of

**↖↖ These are not the final page numbers!**

Table 2. Atomic coordinates and equivalent isotropic displacement parameters [pm²] for Ba$_2$[Ni$_3$N$_2$] at 293 K, 200 K, and 100 K. The Ni(2) atom is described with a split position. Standard deviations of the last digit are in parentheses.

| Temperature | Atom | Site | $x$ | $y$ | $z$ | $U_{eq}$ | Occupancy |
|---|---|---|---|---|---|---|---|
| 293 K | Ba(1) | 8 f | 0 | 0.168902(15) | 0.090882(17) | 99.9(6) | 1 |
| | Ni(1) | 8 e | 0.25 | 0.42484(3) | 0.25 | 83.6(8) | 1 |
| | Ni(2) | 8 d | 0.0207(5) | 0.5 | 0 | 106(5) | 0.5 |
| | N(1) | 8 f | 0 | 0.4259(2) | 0.2298(3) | 82(4) | 1 |
| 200 K | Ba(1) | 8 f | 0 | 0.169011(14) | 0.090908(18) | 74.3(6) | 1 |
| | Ni(1) | 8 e | 0.25 | 0.42493(3) | 0.25 | 65.5(7) | 1 |
| | Ni(2) | 8 d | 0.0200(4) | 0.5 | 0 | 87(4) | 0.5 |
| | N(1) | 8 f | 0 | 0.4256(2) | 0.2300(3) | 67(3) | 1 |
| 100 K | Ba(1) | 8 f | 0 | 0.169150(14) | 0.090764(17) | 34.6(5) | 1 |
| | Ni(1) | 8 e | 0.25 | 0.42508(3) | 0.25 | 33.2(7) | 1 |
| | Ni(2) | 8 d | 0.0205(4) | 0.5 | 0 | 51(4) | 0.5 |
| | N(1) | 8 f | 0 | 0.4260(2) | 0.2301(3) | 42(3) | 1 |

Table 3. Anisotropic displacement parameters [pm²] for Ba$_2$[Ni$_3$N$_2$] at 293 K, 200 K, and 100 K. The Ni(2) atom is described with a split position. Standard deviations of the last digit are in parentheses.

| Temperature | Atom | $U_{11}$ | $U_{22}$ | $U_{33}$ | $U_{23}$ | $U_{13}$ | $U_{12}$ |
|---|---|---|---|---|---|---|---|
| 293 K | Ba(1) | 131.5(9) | 79.0(9) | 89.2(8) | −9.9(5) | 0 | 0 |
| | Ni(1) | 37.5(14) | 103.5(16) | 109.7(13) | 0 | 3.2(11) | 0 |
| | Ni(2) | 135(15) | 109(2) | 75(2) | 16.1(18) | 0 | 0 |
| | N(1) | 47(9) | 103(10) | 94(10) | 9(7) | 0 | 0 |
| 200 K | Ba(1) | 92.9(8) | 67.4(8) | 62.6(7) | −6.5(4) | 0 | 0 |
| | Ni(1) | 28.6(13) | 87.9(14) | 80.1(12) | 0 | 2.8(10) | 0 |
| | Ni(2) | 123(13) | 84(2) | 55(2) | 10.4(15) | 0 | 0 |
| | N(1) | 42(8) | 105(9) | 53(7) | 11(6) | 0 | 0 |
| 100 K | Ba(1) | 43.7(7) | 33.3(7) | 26.6(7) | −3.5(4) | 0 | 0 |
| | Ni(1) | 10.8(13) | 49.0(13) | 39.8(11) | 0 | 0.4(10) | 0 |
| | Ni(2) | 85(12) | 43(2) | 25.0(18) | 6.2(15) | 0 | 0 |
| | N(1) | 23(8) | 73(8) | 31(7) | 8(6) | 0 | 0 |

Table 4. Selected lengths and bond angles in Ba$_2$[Ni$_3$N$_2$] at 293 K, 200 K, and 100 K. Standard deviations of the last digit are in parentheses.

| Temperature | Atoms | Distance [pm] | No. of bonds | Atoms | Distance [pm] | No. of bonds | Atoms | Angle [°] |
|---|---|---|---|---|---|---|---|---|
| 293 K | Ni(1)−N | 179.45(5) | 2 × | N−Ni(1) | 179.45(5) | 2 × | N-Ni(1)-N | 179.30(1) |
| | Ni(2)−N | 187.1(2) | 2 × | N−Ni(2) | 187.1(2) | 1 × | N-Ni(2)-N | 170.92(10) |
| | Ni(2)−Ni(2) | 29.6(7) | | N−Ba | 283.9(2) | 1 × | | |
| | Ni(1)−Ni(2) | 259.2(2) | 2 × | N−Ba | 284.6(2) | 1 × | | |
| | Ni(1)−Ni(2) | 278.9(3) | 2 × | N−Ba | 284.7(2) | 1 × | | |
| | | | | Ba−N | 284.7(2) | 1 × | | |
| | | | | Ba−N | 284.6(2) | 1 × | | |
| | | | | Ba−N | 283.9(2) | 1 × | | |
| 200 K | Ni(1)−N | 178.73(5) | 2 × | | | | | |
| | Ni(2)−N | 186.3(2) | 2 × | | | | | |
| | Ni(2)−Ni(2) | 28.5(6) | | | | | | |
| 100 K | Ni(1)−N | 178.74(5) | 2 × | | | | | |
| | Ni(2)−N | 186.2(2) | 2 × | | | | | |
| | Ni(2)−Ni(2) | 29.2(5) | | | | | | |

170.46(1)° shows an explicit kink giving rise to a zigzag chain nearly planar in the (010) plane, the Ni(1) atom is located about 1.0(1) pm above this plane constituted by the N atom. Neighboring NiN$_{2/2}$ chains are connected through the Ni(2) atom in alternating directions [001] and [00$\bar{1}$] at every

other N atom with the Ni(2) atom statistically occupying a split position.

The description of the 2D complex anion [Ni$_3$N$_2$$^{4-}$] (see Figure 2a) focuses on a (corrugated) square net of Ni(1) atoms (dotted lines in Figure 2a). The (Ni(1)$_2$−Ni(2)−
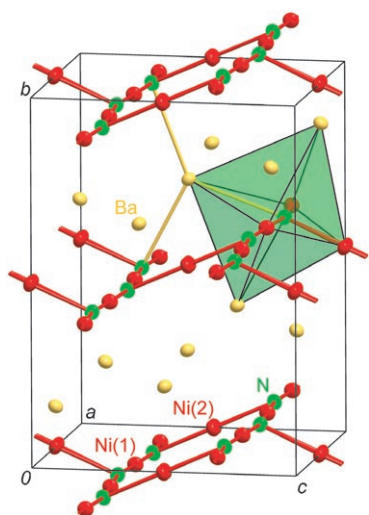
**These are not the final page numbers!** ⬈⬈

Figure 1. Section of the crystal structure of $Ba_2[Ni_3N_2]$. Unit cell and co-ordination spheres of Ba, Ni, and N are highlighted.
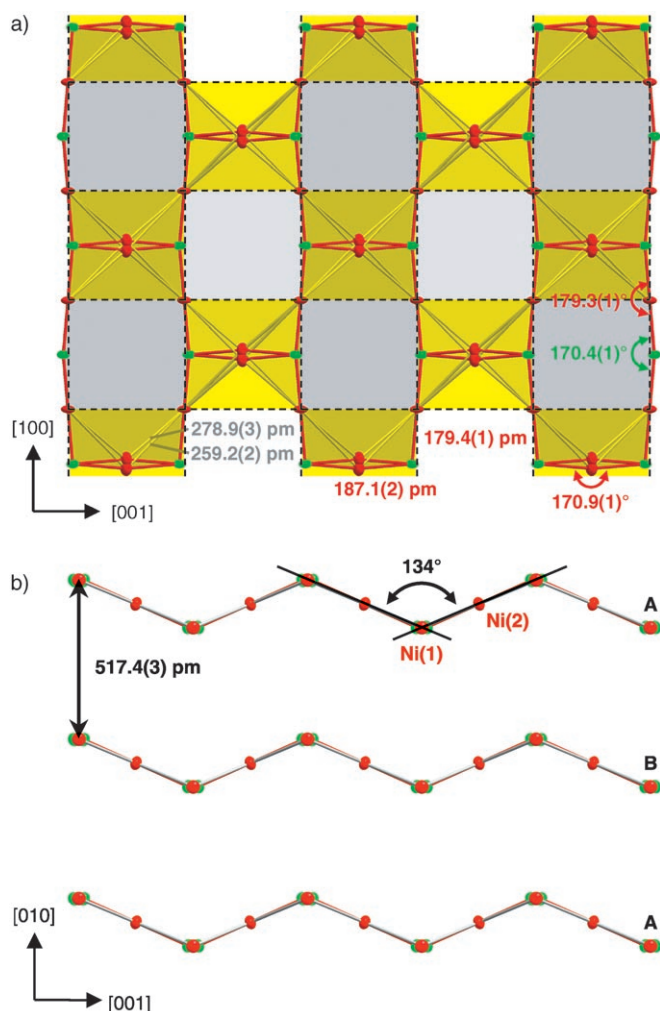


Figure 2. a) $_\infty^2[Ni_3N_2^{4-}]$ anionic layer, Ni(1) square net (dotted lines) and $Ni(1)_2Ni(2)Ni(1)_2$ squares (yellow) highlighted, corrugation indicated by light and dark gray shading. b) Stacking sequence of layers $_\infty^2[Ni_3N_2^{4-}]$.

$(Ni(1)_2)$ units (yellow squares in Figure 2a) are planar, which gives rise to planar bands of Ni(1) squares alternatingly centered by a Ni(2) atom or being empty along the [100] direction. Ni(1)–Ni(2) distances (259.2(2) and 278.9(3) pm) correspond well with data of other nitridonickelates (Sr[NiN]: $d(Ni-Ni) = 237.6$ pm;[6] Ba[NiN]: $d(Ni-Ni) = 242.6$ pm;[7] $Ba_2(Ba_6N)[NiN]_6N$: $d = 256.8$ pm[8]). The N atoms are located on the edges of these planar bands. The angle between the interconnected bands is 134(1)° resulting in a corrugated layer $_\infty^2[Ni_3N_2^{4-}]$ (see Figure 2b). By assuming a purely formal ionic situation, $Ba_2[Ni_3N_2]$ may be described as mixed-valent $Ba_2[Ni^I_2Ni^0N_2]$.

The anomaly in the anisotropic displacement parameters for the Ni(2) atom was studied as part of a detailed investigation of the low-temperature behavior of the crystal structure of $Ba_2[Ni_3N_2]$. Close investigation of both room-temperature and low-temperature X-ray diffraction data did not reveal any superstructure reflections or violations of reflection conditions. To distinguish between dynamic ("cigar-shaped" thermal vibrations) and static displacement (Ni(2) split position), low-temperature single-crystal X-ray diffraction data were collected at temperatures of 200 and 100 K. Refinements of these data clearly validate the split-position model, as is shown in Figure 3. Whereas the cross section of
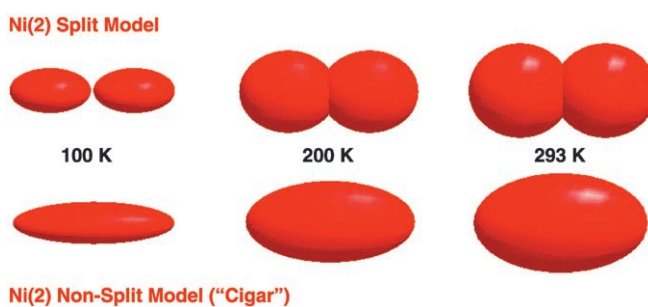


Figure 3. Temperature dependence of the thermal displacement ellipsoids of the Ni(2) position; top: split position (0.02, 0.5, 0), bottom: "ideal" non-split position (0, 0.5, 0).

the thermal displacement ellipsoid in the "idealized" model (Ni(2) in (0.0,5,0)) steadily decreases with decreasing temperature, the longest axis of the thermal displacement ellipsoid remains constant indicating a clear inconsistency in the model. In contrast, in the split-position model (Ni(2) in (0.02,0.5,0)) the thermal displacement ellipsoid isotropically decreases with decreasing temperature, whereas the Ni(2)–Ni(2) interatomic distance remains virtually constant (29(2) pm).

To discuss the split position of the Ni(2) atom in more detail, group–subgroup relations were taken into consideration. The space group $Cmca$ has 15 maximal nonisomorphic subgroups,[16] but in only four of the subgroups ($C222_1$ (no. 20), $C2ca$ (no. 41), $Pbcb$ (no. 54), $Pbna$ (no. 60)) the split-position Ni(2) atom is resolved into two independent positions Ni(2a) and Ni(2b) (Figure 4). In the 11 other maximal

**These are not the final page numbers!**
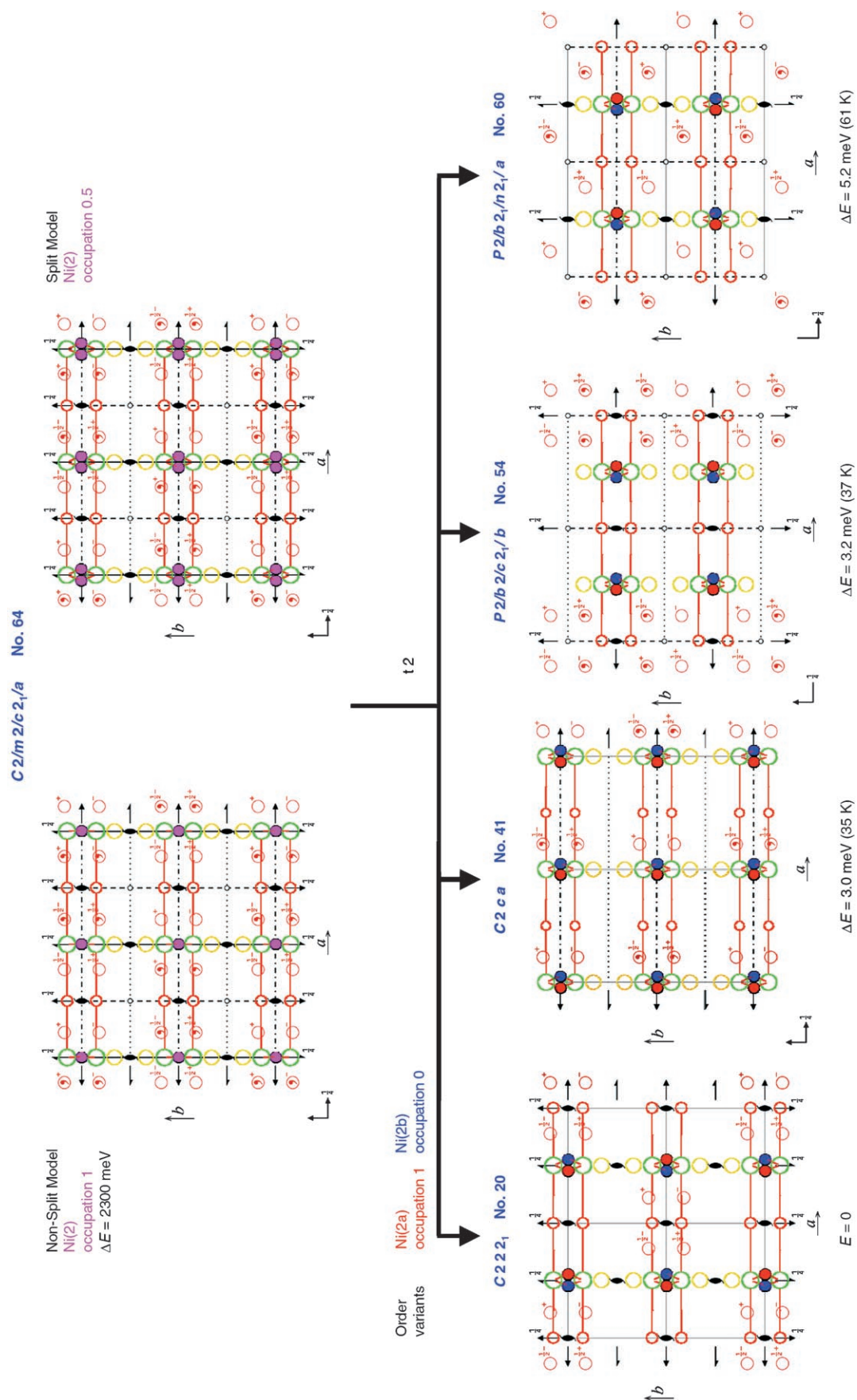
Figure 4. Group–subgroup relationships in Ba$_2$[Ni$_3$N$_2$]. Only the four maximal non-isomorphic subgroups are shown that allow an ordering of Ni(2).

These are not the final page numbers! ↗↗

non-isomorphic subgroups the split-position Ni(2) atom remains unaltered due to symmetry restrictions.[17] Data refinement in any of these four subgroups does not improve the crystal structure description, but always results in twin models that resemble the Ni(2) atom split position. Since there are no indications of macroscopic twinning, we must assume that either "real" disorder is prevalent or ordered microstructural domains are present. For a deeper insight into this we performed electronic structure calculations.

**Electronic structure calculations:** Starting from the description of $Ba_2[Ni_3N_2]$ in the space group *Cmca* (no. 64) with the Ni(2) atom in the center of the large thermal displacement ellipsoid, we performed total energy calculations for the four different ordered occupation patterns shown in Figure 4 by using the subgroups $C222_1$ (no, 20), *C2ca* (no. 41), *Pbcb* (no. 54), and *Pbna* (no. 60), respectively. We found that the $C222_1$ arrangement exhibited the lowest energy, although the other Ni(2) occupation patterns are very close in energy. Normalized to the energy of the $C222_1$ arrangement, they differ by 3.0 (35 K, *C2ca*), 3.2 (37 K, *Pbcb*), and 5.2 meV (61 K, *Pbna*) per formula unit only. On the other hand, the description in terms of the non-split *Cmca* structure yields an energy of about 2300 meV above the $C222_1$ structure and can therefore be excluded as a stable state at low temperatures. Considering the very small energy differences between the ordered occupation patterns, a long range ordering of the Ni(2) atom split positions is not expected even at low temperatures. The energy barrier between the Ni(2) atom split positions (the *Cmca* energy gives a rough estimate) is more than two orders of magnitude higher than the difference between the different Ni(2) arrangements, therefore, any Ni atom ordering is highly inhibited. Furthermore, the small energy differences between the four Ni(2) patterns will be even further reduced by local relaxation that is neglected in the calculations. That leads us to the conclusion that the Ni(2) atom split position should be completely randomly occupied and corresponds well with the results of the crystal structure refinements.

**Low-temperature investigations:** Low-temperature X-ray powder diffraction data (Figure 5) show an interesting feature: whereas the unit cell volume $V$ and the lattice parameter $b$ decrease steadily as the temperature is lowered, the lattice parameter $a$ (corresponding to the direction of the Ni−N chains) remains almost constant. Above 100 K, the lattice parameter $c$ decreases, but below a transition temperature of $T \approx 100$ K indicating a second order phase transition, the lattice parameter $c$ increases with decreasing temperature, an observation that corresponds to a decreasing corrugation of the $[Ni_3N_2]$ layers with decreasing temperature below 100 K.

Neutron diffraction powder data support the above interpretation (see Figures 6a and b), and no magnetic ordering in the compound could be detected, neither at 298 K (*Cmca* (no. 64), $a = 715.377(11)$, $b = 1031.110(14)$, $c = 739.029(11)$ pm, see Figure 6b) nor at lower temperatures
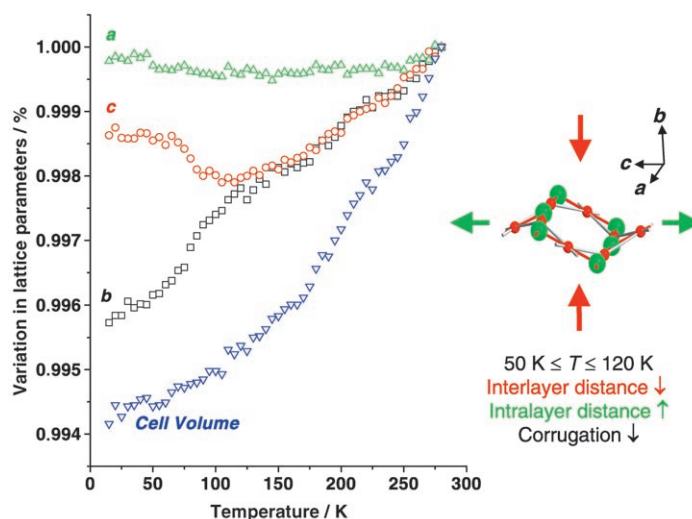


Figure 5. Temperature dependence of lattice parameters and unit cell volume of $Ba_2[Ni_3N_2]$ and its effect on the 2D anion.
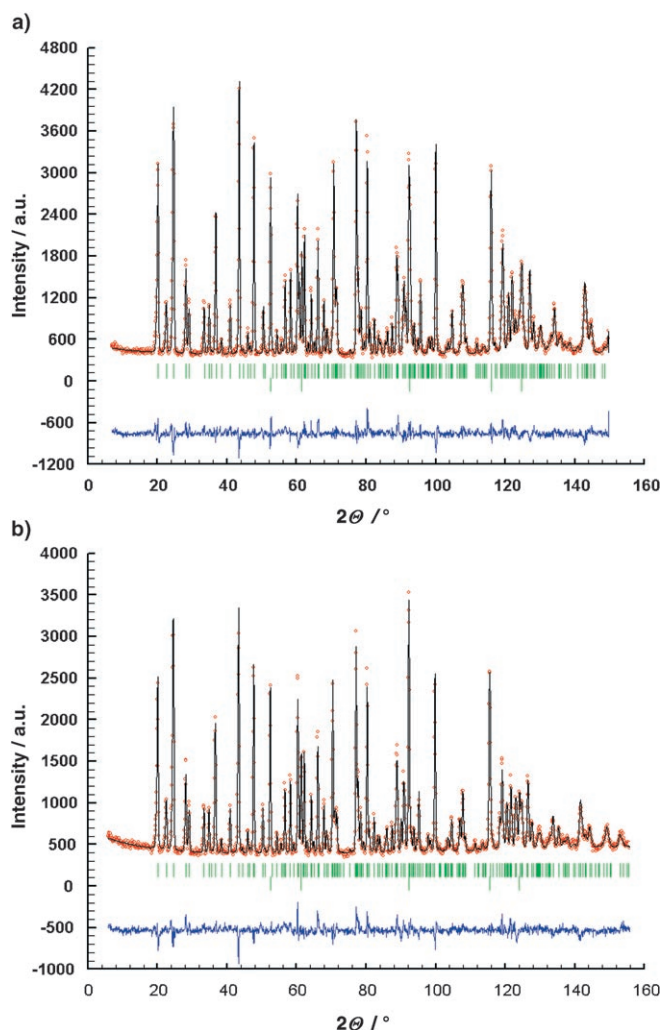


Figure 6. Neutron diffraction refinement of $Ba_2[Ni_3N_2]$ at: a) 2 K and b) 298 K. Tick marks represent $Ba_2[Ni_3N_2]$ (top) and Ni (bottom).

↖↖ These are not the final page numbers!

down to 2 K (*Cmca* (no. 64), $a = 715.606(9)$, $b = 1026.916(11)$, $c = 738.161(9)$ pm, see Figure 6a). Data refinement of powder neutron data with the FULLPROF[18] program package gave results similar to single-crystal X-ray data refinements (Tables 5 and 6).

Table 5. Crystallographic data for Ba$_2$[Ni$_3$N$_2$] at 298 and 2 K from powder neutron diffraction data.

| temperature of measurement | 298 K | 2 K |
|---|---|---|
| crystal system | orthorhombic | |
| space group | *Cmca* (no. 64) | |
| $a$ [pm] | 715.377(11) | 715.606(9) |
| $b$ [pm] | 1031.110(14) | 1026.916(11) |
| $c$ [pm] | 739.029(11) | 738.161(9) |
| cell volume [$10^6$ pm$^3$] | 545.132 (14) | 542.451(11) |
| $Z$ | 4 | |
| crystal color, habit | black, powder | |
| $2\theta$ range [°] | 6–156 | |
| diffractometer | HMI Berlin, E 9 | |
| wavelength [Å] | 1.79685 | |
| independent reflections | 205 | |
| program for structure refinement | FULLPROF[18] | |
| number of parameters | 31 | |
| $R_{\mathrm{Bragg}}$ | 0.079 | 0.059 |
| $R_{\mathrm{Profile}}$ | 0.055 | 0.041 |

Table 6. Atomic coordinates and equivalent isotropic displacement parameters [pm$^2$] from powder neutron diffraction data for Ba$_2$[Ni$_3$N$_2$] at 298 K and 2 K. The Ni(2) atom is described with a split position. Standard deviations of the last digit are in parentheses.

| Temperature | Atom | Site | $x$ | $y$ | $z$ | $B_{\mathrm{iso}}$ | Occupancy |
|---|---|---|---|---|---|---|---|
| 298 K | Ba(1) | 8 f | 0 | 0.1699(6) | 0.0916(6) | 0.81(9) | 1 |
| | Ni(1) | 8 e | 0.25 | 0.4250(3) | 0.25 | 0.61(5) | 1 |
| | Ni(2) | 8 d | 0.0197(15) | 0.5 | 0 | 1.07(10) | 0.5 |
| | N(1) | 8 f | 0 | 0.4254(3) | 0.2293(4) | 0.81(6) | 1 |
| 2 K | Ba(1) | 8 f | 0 | 0.1694(4) | 0.0903(5) | −0.21(6) | 1 |
| | Ni(1) | 8 e | 0.25 | 0.4252(2) | 0.25 | 0.46(4) | 1 |
| | Ni(2) | 8 d | 0.0258(9) | 0.50 | 0.46(8) | 0.5 | |
| | N(1) | 8 f | 0 | 0.4263(2) | 0.2313(3) | 0.52(4) | 1 |

**Electrical resistivity:** The electrical resistivity $\rho(T)$ of Ba$_2$[Ni$_3$N$_2$] (Figure 7) shows a clear linear temperature dependence for $T > 100$ K, indicating a metallic conduction mecha-
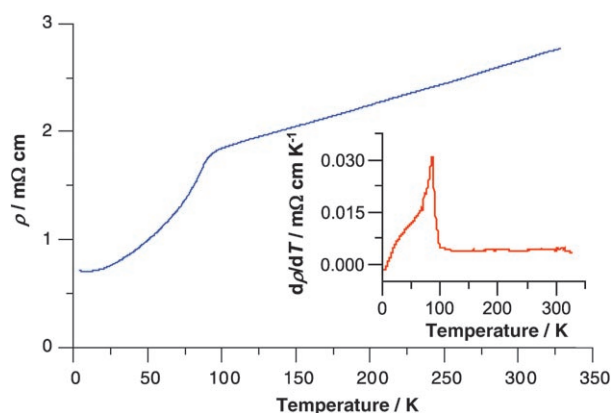


Figure 7. Electrical resistivity of Ba$_2$[Ni$_3$N$_2$] as a function of temperature. The derivative d$\rho$/d$T$ is emphasized in the inset.

nism. However, the resistivity of $\approx 2.7$ m$\Omega$ cm at 300 K is high compared with the classical limit of $\approx 0.1$ m$\Omega$ cm for metallic conduction, classifying the compound as a "poor" metal (similar to the doped cuprate oxides). The crystallographic ($T \approx 100$ K, Figure 5)/magnetic transition ($T \approx 90$ K, Figure 8) is mirrored by a change of the slope of $\rho(T)$ and a strong curvature below that temperature. The derivative d$\rho$/d$T$, which often resembles the temperature dependence of
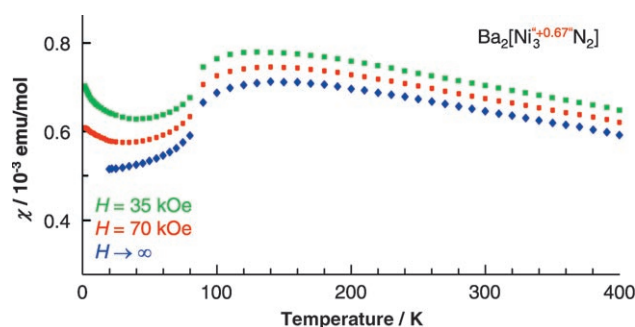


Figure 8. Magnetic susceptibility of Ba$_2$[Ni$_3$N$_2$] against $T$ for different magnetic fields and extrapolation for the pure substance (see text).

the specific heat of magnetic systems, shows a clear $\lambda$ peak at 87 K (inset Figure 7). The shape of d$\rho$/d$T$ is characteristic for the reduction of the spin-disorder scattering of charge carriers in a magnetically ordered phase and therefore may be associated with stronger Ni–Ni interactions due to decreasing corrugation of the 2D network. Interestingly, many alkaline-earth nitridonickelates (Ba[NiN], Ba$_2$(Ba$_6$N)[NiN]$_6$N, and Ba$_2$[Ni$_3$N$_2$]) show "poor" metallic behavior, however, Ba$_2$[Ni$_3$N$_2$] exhibits the lowest resistivity.[19] The solid solution series Li$_2$[(Li$_{1-x}$Ni$_x$)N] reveals an insulator–metal transition with increasing $x$ at $x \approx 0.80$.[20]

**Magnetic susceptibility:** The magnetic susceptibility (Figure 8) of Ba$_2$[Ni$_3$N$_2$] displays a broad maximum around 120 K that is a signature of low-dimensional magnetism. $\chi(T)$ can be approximated by a Curie–Weiss law only at much higher temperature. The effective magnetic moment per formula unit $\mu_{\mathrm{eff}}$/f.u. = 2.5 $\mu_B$ obtained from a linear fit of $1/\chi(T)$ above 200 K is nevertheless roughly consistent with two Ni$^{\mathrm{I}}$ species ($S = 1/2$, $\mu_{\mathrm{so}} = 1.73$ $\mu_B$) on the chain-sites (Ni(1)) and one nonmagnetic Ni$^0$ species in the "connection-site" (Ni(2)). However, as shown above, the system is metallic and the situation is clearly not in the ionic limit with well-defined magnetic moments localized at certain Ni species. The magnetic system might be therefore described as Ni-centered quantum spins ($S = 1/2$) with predominant

**These are not the final page numbers!** ↗↗

magnetic exchange in the chains running in the *a* direction. The sharp kink in $\chi(T)$ at $T_N \approx 90$ K and the concomitant strong reduction of the electrical resistivity indicate the long-range antiferromagnetic ordering of the Ni species. The fact, that no additional reflections were observed in the neutron diffraction powder data at low temperature ($T = 2$ K) might be due to a very small ordered magnetic moment. This situation is often met in low-dimensional isoelectronic copper $S = \frac{1}{2}$ compounds. The relatively high $T_N$ compared to the temperature of the maximum in $\chi(T)$ indicates a strong out-of-chain coupling (along the *c* axis). Magnetic coupling along the *b* axis can be quite weak in this respect. The spin quantum number $\frac{1}{2}$ and the coupling to a structural distortion render this compound a very interesting magnetic system. There is no significant shift or broadening of the phase transition due to the high applied magnetic field. Field or temperature hysteresis effects were also not detected. Thus no weak ferromagnetic moments at 90 K or other phase transitions have been observed for $T > 1.8$ K.

**X-ray absorption spectroscopy:** For independent information on the electronic states of nickel, X-ray absorption spectroscopy was employed at the *K*-threshold of Ni. XAS spectra of $Ba_2[Ni_3N_2]$ were collected at different temperatures between 5 and 300 K. Representative spectra at 5, 100, and 300 K along with the spectra of $Ni^0$ and $Ni^{II}O$ as energy references are shown in Figure 9a. The derivative of the Ni *K*-edge X-ray absorption spectrum is shown in Figure 9b. The X-ray absorption spectrum of $Ba_2[Ni_3N_2]$ shows several contributions of varying magnitude to the fine-structure near to the Ni *K*-edge. These secondary peaks are more visible from the derivative curve, which shows at least four distinct maxima in the edge region. The energies as well as the shapes of these features are temperature independent that is shown by the spectra and their derivatives at $T = 5$ and 300 K, and agree well also with spectra near the phase transition at 100 K.

The comparison of the absorption spectra of $Ba_2[Ni_3N_2]$ with spectra of Ni and NiO used as $Ni^0$ and $Ni^{II}$ references show stronger similarities to the Ni spectrum with respect to position and shape of the *K*-edges indicating a low Ni electronic state of $Ba_2[Ni_3N_2]$. Major differences to the spectrum of elemental Ni occur near to the first maximum, the magnitude of which is reduced and not well-defined in the $Ba_2[Ni_3N_2]$ spectrum. This absorption maximum is related to the main contribution of the density of states at the Ni *K*-edge and is caused by the dipole excitation of 1s electrons to unoccupied 4p levels above the Fermi energy. This relation of the absorption behavior at the *K*-edge to the $l = 1$ projected density of states was calculated for $Ni^{[21]}$ and $NiO$.[22] Both spectra and their first derivatives show the main maximum at almost the same energy. In the low-energy region the absorption of elemental Ni is significantly higher than for NiO, which reflects the differences in the $l = 1$ projection of the density of states above the Fermi energy. The absorption behavior of both elemental Ni and $Ba_2[Ni_3N_2]$ is very similar in the low-energy region. For elemen-
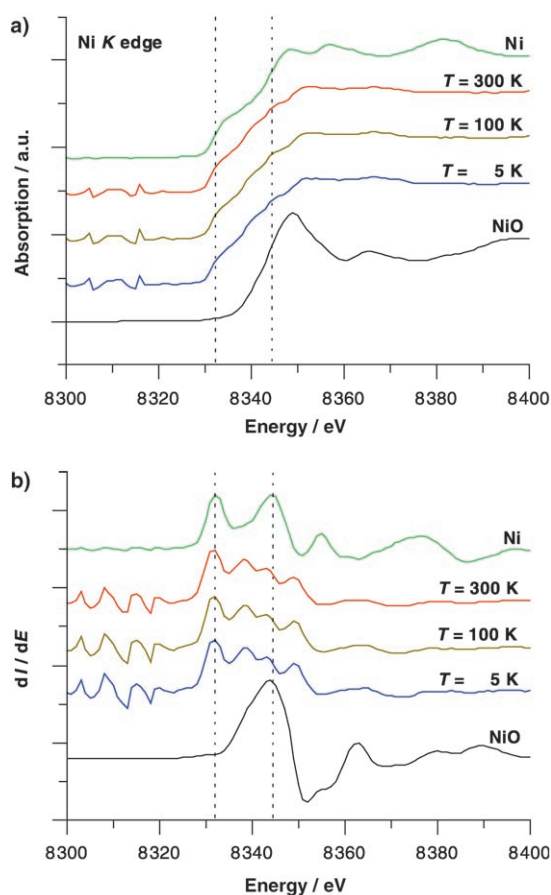


Figure 9. a) Ni *K*-edge X-ray absorption spectra of $Ba_2[Ni_3N_2]$ at different temperatures, $Ni^0$, and $Ni^{II}O$. b) Derivative curve of Ni *K*-edge X-ray absorption spectra of $Ba_2[Ni_3N_2]$ at different temperatures, $Ni^0$, and $Ni^{II}O$.

tal Ni, it was found that the absorption behavior is dominated by contributions of unoccupied 3d levels on the $l = 1$ projection of the density of states in this energy range. The coincidence of both spectra in this energy range indicates similar 3d level configurations for elemental Ni and $Ba_2[Ni_3N_2]$. This relation will be further investigated by theoretical calculations of the absorption coefficient that should also give some hints on the differences arising from the Ni configurations in both elemental Ni and $Ba_2[Ni_3N_2]$ due to the varying absorption behavior near the first maximum.[23]

Qualitatively, the absorption spectra of $Ba_2[Ni_3N_2]$ do not change with temperature and show that the $l = 1$ projection of the density of states is temperature independent. This indicates that the phase transition at 100 K is not related to changes in the band structure of the compound or to major changes near the Fermi energy.

## Conclusion

$Ba_2[Ni_3N_2]$ exhibits the lowest average oxidation state of Ni ($+0.67$) observed in nitridonickelates so far. The mixed-valent nickel compound contains a two-dimensional com-

**⤺⤺ These are not the final page numbers!**

plex anion that is built up by Ni(1)−N chains connected by N-Ni(2)-N dumb-bell units. The split position of the nearly linearly coordinated Ni(2) atom is discussed taking group–subgroup relations into account using both diffraction data and FPLO calculations. Ba$_2$[Ni$_3$N$_2$] is a "poor" metal and displays a structural and magnetic phase transition at $T \approx 90$ K. The transition is interpreted as a long range antiferromagnetic ordering of Ni$^I$ species accompanied by a symmetry-retaining structural distortion. XAS investigations correspond well with the low oxidation state of Ni and corroborate the electric and magnetic measurements.

## Experimental Section

Owing to the high sensitivity towards air and moisture of the compounds of the system under investigation, all manipulations were performed inside an argon-filled glovebox ($p(O_2, H_2O) < 0.1$ ppm). Temperature experiments were performed using a quartz-glass tube reactor and a tube furnace capable of sustaining temperatures up to 1423 K. The sample purity was checked by powder X-ray diffraction methods and by elemental analysis.

Ba$_2$N as a starting material was prepared by the reaction of dendritic barium metal (Alfa, 99.987 %) with nitrogen of ambient back-pressure (Messer–Griesheim, 99.999 %, additionally purified by passing over molecular sieve, Roth 3 Å, and BTS catalyst, Merck), in a tantalum crucible placed inside a quartz-glass tube reactor by heating for 48 h at 923 K. To prevent a reaction of the quartz reactor with subliming Ba$_2$N, the tantalum crucible was placed inside a stainless steel tube. To remove diazenide impurities in the Ba$_2$N, the sample was heated under vacuum at 673 K for 12 h. The Ba$_2$N thus prepared was black, ductile, and shone with a metallic luster. Its quality was ascertained by X-ray powder diffraction and elemental analysis. Nickel powder (100 mesh, Chempur, 99.9 %) was used without further purification after ascertaining its purity by X-ray powder diffraction measurement and elemental analysis.

For the preparation of dark gray single-phase Ba$_2$[Ni$_3$N$_2$], a mixture of Ba$_2$N and Ni (molar ratio 1.00:3.00) was ground to a fine powder and pelletized. The pellets were sintered in a nickel crucible placed in the quartz reactor described above under an ambient back-pressure of nitrogen at 1173 K for 240 h. Sintering with intermediate regrinding and repelletizing was repeated until complete reaction was achieved. Irregular-shaped, black single crystals with metallic luster were prepared by heating a mixture of Ba$_2$N and Ni (molar ratio 1.00:2.50) in a nickel crucible under an ambient back-pressure of nitrogen at 1273 K for 36 h. Ba$_2$[Ni$_3$N$_2$] is sensitive towards air and moisture.

The chemical composition of Ba$_2$[Ni$_3$N$_2$] was checked by elemental analysis of the bulk material. The N and O content was determined quantitatively by a carrier-gas hot-extraction technique (LECO analyzer TC-436 DR/5), no oxygen impurities above the detection limit (typically 15 mg powder sample, $<0.02$ % oxygen on weight) were found. The Ni and Ba content was determined quantitatively using ICP-OES (Varian "Vista RL" radial plasma). All values corresponded well with calculated data. Elemental analysis calcd (%) for Ba$_2$[Ni$_3$N$_2$]: Ba 57.28, Ni 36.87, N 5.84; found: Ba 56.6(1.4), Ni 37.9(1.1), N 5.66(4).

For X-ray powder diffraction investigations the samples were ground to a very fine powder and evenly distributed between two Kapton films for protection against air and moisture. Measurements were performed on a Huber image-plate Guinier camera in the $2\theta$ range of 3–100° (exposure time 90 min), using Cu$_{K\alpha1}$ radiation. Low-temperature X-ray powder diffraction data collection ($10 = T = 300$ K) was performed by using the same setup with the sample placed inside a closed-cycle helium cryostat.

Suitably sized single crystals of Ba$_2$[Ni$_3$N$_2$] were sealed in glass capillaries for X-ray diffraction intensity data collection on a STOE IPDS automatic four-circle diffractometer with Ag$_{K\alpha}$ radiation using a graphite-monochromator and the $\varphi$ scan technique. An open nitrogen gas stream as coolant was employed for low-temperature single-crystal X-ray diffraction measurements. The crystal structure was solved from single-crystal data and was refined by using the SHELX software package.[24]

Neutron diffraction experiments were carried out on the powder diffractometer E9 at the BER II reactor of the Hahn–Meitner Institute (HMI), Berlin, Germany. Ba$_2$[Ni$_3$N$_2$] ($\approx 3$ g) was placed under argon into a cylindrical vanadium container (diameter 6 mm, length 47 mm, and wall thickness 0.15 mm) closed with a cap containing an indium seal. Crystal structure data were derived from neutron diffraction experiments with the wavelength $\lambda = 1.79685(2)$ Å in the range $2 < 2T < 158°$ at 298 and 2 K. The refinements were carried out using the FULLPROF[18] and GSAS[25] programs.

Magnetization measurements at different magnetic fields between 100 Oe and 70 kOe in the temperature range 2–400 K were carried out in a SQUID magnetometer (MPMS XL-7, Quantum Design). The polycrystalline sample ($\approx 100$ mg) was sealed in a quartz tube under 0.4 bar He atmosphere. Corrections for the sample container were applied. Owing to traces of ferromagnetic nickel metal impurities ($\approx 60$ ppm by mass) in the sample a correction of the high-field data ($\chi(T)$ versus $1/H$ extrapolated to 0, Honda–Owen method) was utilized to obtain the intrinsic susceptibility of the compound.

Electrical resistivity measurements were performed on phase-pure (ascertained by X-ray powder diffraction data) powder in situ pressed to a cylindrical tablet in a sapphire die cell. The van-der-Pauw method with four soft Pt spheres as electrical contacts pressed into the sample was utilized in the temperature range 4–320 K. All manipulations and measurements were carried out inside an argon-filled glovebox with an integrated cryostat.

X-ray absorption spectra (XAS) at the $K$-threshold of nickel were collected to obtain information on the electronic state of nickel. The powder samples were mixed with B$_4$C in a volume ratio of 1:3 to produce a homogeneous absorber. To prevent contamination from moisture and air the sample was loaded in a steel capsule, equipped with Be-windows (0.5 mm). For low-temperature (5 K $\leq T \leq$ 300 K) XAS measurements the sample preparation was modified: a mixture of Ba$_2$[Ni$_3$N$_2$] and B$_4$C was added to molten dry paraffin, the mixture was cast into an appropriately sized die, and upon solidification was wrapped with Kapton foil to prevent contamination by moisture and air. The measurements were performed at the A1 bending magnet beam-line located at the DORIS III storage-ring in the HASYLAB, DESY Laboratory (Hamburg, Germany). The X-ray beam was monochromatized using a double-crystal monochromator equipped with a Si(111) crystal. The Ni $K$-edge measurements were performed in transmission geometry. The absorption spectra of the compound were measured simultaneously with the spectrum of nickel foil serving as a reference for energy calibration.

**Electronic structure calculations:** To investigate the nature of the occupation patterns for the Ni(2) split position of the N-Ni(2)-N dumb-bell, full-potential electronic structure calculations within the local density approximation (LDA) were carried out. For this purpose an FPLO calculation scheme[26] was applied. In the scalar-relativistic calculations the exchange and correlation potential of Perdew and Wang[27] was used. As the basis set, Ba (5s, 5p, 6s, 6p, 5d), Ni (3s, 3p, 4s, 4p, 3d), and N (2s, 2p, 3d) states were employed. The lower-lying states were treated fully relativistically as core states. The N (3d) and the Ba (5d) states were taken into account as polarization states to increase the completeness of the basis set and thus the accuracy of the total energy. The treatment of the Ni (3s, 3p) and Ba (5s, 5p) semi-core-like states as valence states was necessary to account for non-negligible core–core overlaps. The spatial extension of the basis orbitals, controlled by a confining potential $(r/r_0)^4$, was optimized to minimize the total energy.[28] A $k$-mesh of 4096 points in the full Brillouin zone was used. The convergency of the total energy with respect to the $k$-mesh and the basis set was carefully checked.
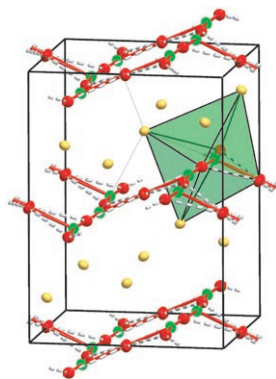
[1] R. Kniep, *Pure Appl. Chem.* **1997**, *69*, 185–191; R. Niewa, H. Jacobs, *Chem. Rev.* **1996**, *96*, 2053–2062.

[2] W. Sachsze, R. Juza, *Z. Anorg. Allg. Chem.* **1949**, *259*, 278–290.

[3] M. Y. Chern, F. J. DiSalvo, *J. Solid State Chem.* **1990**, *88*, 459–464.

[4] A. Gudat, R. Kniep, J. Maier, *J. Alloys Compd.* **1992**, *186*, 339–345.

[5] A. Gudat, R. Kniep, A. Rabenau, *Thermochim. Acta* **1990**, *160*, 49–56.

[6] T. Yamamoto, S. Kikkawa, F. Kanamaru, *J. Solid State Chem.* **1995**, *115*, 353–359.

[7] A. Gudat, S. Haag, R. Kniep, A. Rabenau, *J. Less-Common Met.* **1990**, *159*, L29 L31.

[8] A. Gudat, W. Milius, S. Haag, R. Kniep, A. Rabenau, *J. Less-Common Met.* **1991**, *168*, 305–312.

[9] A. Gudat, R. Kniep, A. Rabenau, *Z. Anorg. Allg. Chem.* **1991**, *597*, 61–67.

[10] A. Gudat, R. Kniep, A. Rabenau, *Z. Anorg. Allg. Chem.* **1992**, *607*, 8–12.

[11] J. Klatyk, P. Höhn, R. Kniep, *Z. Kristallogr. New Cryst. Struct.* **1998**, *213*, 31.

[12] M. G. Barker, A. J. Blake, P. P. Edwards, D. H. Gregory, T. A. Hamor, D. J. Siddons, S. E. Smith, *Chem. Commun.* **1999**, *13*, 1187–1188.

[13] G. R. Kowach, N. E. Brese, U. M. Bolle, C. J. Warren, F. J. DiSalvo, *J. Solid State Chem.* **2000**, *154*, 542–550.

[14] P. Höhn, A. Mehta, R. Kniep, unpublished results.

[15] A. Mehta, P. Höhn, R. Kniep, *Z. Anorg. Allg. Chem.* **2002**, *628*, 2173.

[16] *International Tables for Crystallography. Vol. A* (Ed.: Th. Hahn), Kluwer Academic Publishers, Dordrecht, The Netherlands, **1996**.

[17] H. Bärnighausen, *Match* **1980**, *9*, 139–175.

[18] J. Rodriguez-Carvajal, Laboratoire Leon Brillouin, Saclay, FULL-PROF.2 K (Version 2.45), July **2003**.

[19] P. Höhn, A. Mehta, W. Schnelle, R. Kniep, unpublished results.

[20] W. Schnelle, R. Niewa, F. R. Wagner, *J. Magn. Magn. Mater.* **2004**, *828*, 272–276.

[21] J. E. Müller, O. Jepsen, J. W. Wilkins, *Solid State Commun.* **1982**, *42*, 365–368.

[22] H. Modrow, S. Bucher, J. J. Rehr, and A. L. Ankudinov, *Phys. Rev. B* **2003**, 67, 035123.

[23] H. Rosner, P. Höhn, unpublished results.

[24] G. M. Sheldrick, SHELXL97–2, University of Göttingen, Göttingen, Germany, **1997**.

[25] A. C. Larson and R. B. Von Dreele, "General Structure Analysis System (GSAS)", Los Alamos National Laboratory Report LAUR 86–748, **2000**, and B. H. Toby, EXPGUI, A Graphical User Interface for GSAS, *J. Appl. Crystallogr.* **2001**, *34*, 210.

[26] K. Koepernik, H. Eschrig, *Phys. Rev. B* **1999**, *59*, 1743.

[27] J. P. Perdew, Y. Wang, *Phys. Rev. B* **1992**, *45*, 13 244.

[28] H. Eschrig, *Optimized LCAO Method and the Electronic Structure of Extended Systems*, Springer, Berlin, **1989**.

**The new ternary alkaline-earth nitrido-nickelate** Ba$_2$[Ni$_3$N$_2$] is the first example of a ternary nitridonickelate with a two-dimensional complex anion (see picture: Ba yellow, Ni red, N green). The average oxidation state of Ni is +0.67, the lowest mean value observed in nitridonickelates so far. The assignment of different crystallographic Ni positions to the unusually low oxidation states Ni$^0$ and Ni$^1$ is discussed using full-potential nonorthogonal local-orbital (FPLO) methods and taking the physical properties into account.

These are not the final page numbers! ↗↗